
Longitudinal Variational Autoencoder

Siddharth Ramchandran¹ Gleb Tikhonov¹ Miika Koskinen^{2,3} Harri Lähdesmäki¹

¹Department of Computer Science, Aalto University, Finland

²Helsinki Biobank, HUS Helsinki University Hospital, Finland

³Faculty of Medicine, University of Helsinki, Finland

{siddharth.ramchandran, gleb.tikhonov, harri.lahdesmaki}@aalto.fi

Abstract

Longitudinal datasets measured repeatedly over time from individual subjects, arise in many biomedical, psychological, social, and other studies. Such multivariate time-series are often high-dimensional and contain missing values. A common approach to analyse this kind of data is to learn a low-dimensional representation using variational autoencoders (VAEs). However, standard VAEs assume that the learned representations are i.i.d., and fail to capture the correlations between the data samples. We propose a novel deep generative model, Longitudinal VAE (L-VAE), that uses a multi-output additive Gaussian process (GP) prior to extend the VAE's capability to learn structured low-dimensional representations imposed by auxiliary covariate information, and also derive a new divergence upper bound for such GPs. Our approach can simultaneously accommodate both time-varying shared and random effects, produce structured low-dimensional representations, disentangle effects of individual covariates or their interactions, and achieve highly accurate predictive performance. We compare our model against previous methods on synthetic and clinical datasets, and demonstrate the state-of-the-art performance in data imputation, reconstruction, and long-term prediction tasks.

1 Introduction

Longitudinal datasets naturally arise in a wide variety of fields and applications, such as biomedicine, sociology, psychology and many others. Such datasets include, for example healthcare records, social media behaviour, consumer behaviour, students' grades during their studies, etc., all collected repeatedly over time for each individual. Most longitudinal datasets contain both dependent and independent variables. For example, in biomedical data, dependent variables can comprise of lab test measurements and other vital measurements of the patient, such as blood sugar levels, heart rate, body temperature, etc., whereas independent variables contain additional auxiliary descriptors of the patient, such as age, sex, time to disease event, measurement times, etc. Analysing longitudinal datasets collected in such studies is challenging as they often involve time-varying covariates, high-dimensional correlated outcome values, and missing values.

While non-linear, high-dimensional generative models are capable of learning complex data distributions, the statistical inference and training for such models is generally highly non-trivial. Auto-Encoding Variational Bayes (AEVB) (Kingma and Welling, 2013) is a powerful deep learning technique that provides an efficient inference method for latent variable models. The variational autoencoder (VAE), the most popular exemplification of AEVB, learns a low-dimensional latent code of the dataset using two complementary deep neural networks (DNNs) to encode the high-dimensional data and decode the latent distribution, respectively. However, VAEs usually ignore the possible correlations (e.g. temporal correlations) between the learnt latent embeddings.

Related work Numerous extensions have been proposed for VAEs. Kulkarni et al. (2015) proposed to group samples with specific properties in mini-batches to induce structure on the latent space. The conditional VAE (CVAE) of Sohn et al. (2015) incorporated the auxiliary covariate information directly in the inference and generative networks. Limitations of the expressiveness of posterior approximations in VAEs has been addressed by using normalising flows (NF) (Rezende and Mohamed, 2015) implemented with RealNVPs (Dinh et al., 2016), continuous-time NFs (Chen et al., 2017), and importance sampling (Müller et al., 2018). Methods have also been proposed to handle the disentanglement of dimensions in the latent space (Ainsworth et al., 2018a,b; Higgins et al., 2017). All these methods, however, assume independence across samples. Casale et al. (2018) proposed to incorporate auxiliary information in a Gaussian process (GP) prior to model the VAE’s latent space structure. Fortuin et al. (2019) built upon this idea and described an extension that can model time series data and accounts for missing values.

GPs enable flexible probabilistic time-series modelling and incorporate prior knowledge or beliefs through the use of appropriate covariance functions (Williams and Rasmussen, 2006). GPs can be extended to high-dimensional data (Alvarez et al., 2011) and latent variable modelling with auxiliary information by combining GPs with GPLVMs (Märtens et al., 2018). In the context of deep learning, recurrent neural networks (RNNs), such as BRITS (Cao et al., 2018) are well-suited to temporal data. However, the RNN model structure is inherently limited to evenly sampled data, and incorporating additional auxiliary information is not straightforward. For time-series data imputation, recurrent models have also been trained using the generative adversarial networks (GANs) (Luo et al., 2018).

Contribution In this paper, we propose a novel deep generative model that extends the capabilities of a VAE with a multi-output additive GP prior over the latent encodings, that model the correlation structure between the samples w.r.t. auxiliary information. Our L-VAE model is conceptualised in fig. 1. Our model probabilistically encodes the longitudinal measurements with missing values onto a low-dimensional latent space with no missing values. The structured, low-dimensional latent dynamics are modelled using a multi-output additive GP that utilises the auxiliary covariates, followed by decoding back to the data domain. The multi-output additive GP prior introduces computational challenges for which we derive a divergence bound that leverages the commonly used inducing point formalism (Quiñonero-Candela and Rasmussen, 2005; Titsias, 2009) for efficient model inference. Our contributions can be summarised as follows:

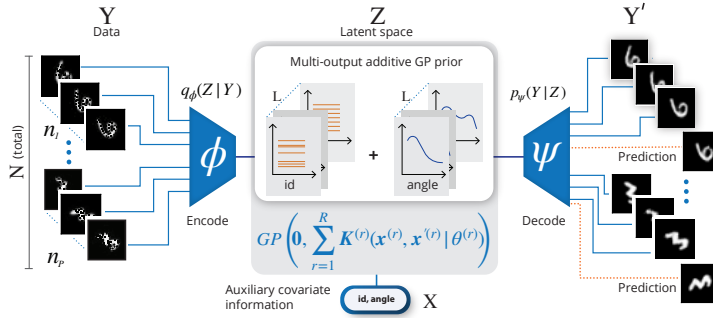


Figure 1: L-VAE overview.

values. The structured, low-dimensional latent dynamics are modelled using a multi-output additive GP that utilises the auxiliary covariates, followed by decoding back to the data domain. The multi-output additive GP prior introduces computational challenges for which we derive a divergence bound that leverages the commonly used inducing point formalism (Quiñonero-Candela and Rasmussen, 2005; Titsias, 2009) for efficient model inference. Our contributions can be summarised as follows:

- We introduce a VAE for longitudinal data with auxiliary covariate information, that can model the structured latent space dynamics with a multi-output additive GP prior.
- We derive an efficient approximate GP inference scheme by exploiting the structure of the additive GP covariance functions that are central for longitudinal modelling.
- We compare L-VAE’s performance against competing methods on several datasets and report the state-of-the-art performance in imputation, reconstruction, and long-term prediction.

2 Methods

Problem setting Let D be the dimensionality of the observed data, P be the number of unique instances (e.g. unique patients, unique handwritten digit styles), n_p be the number of longitudinal samples from instance p , and $N = \sum_{p=1}^P n_p$ be the total number of samples (e.g. the total number of measurements for all patients, total number of images). Longitudinal samples for instance p are denoted as $Y_p = [\mathbf{y}_1^p, \dots, \mathbf{y}_{n_p}^p]^T$, where each sample $\mathbf{y}_t^p \in \mathcal{Y} = \mathcal{Y}_1 \times \dots \times \mathcal{Y}_D$ and \mathcal{Y}_d denotes the

domain of the d^{th} feature. In this work, we assume $\mathcal{Y} = \mathbb{R}^D$. We represent the auxiliary covariate information for the instance p as $X_p = [\mathbf{x}_1^p, \dots, \mathbf{x}_{n_p}^p]^T$, where covariates for each sample $\mathbf{x}_t^p \in \mathcal{X} = \mathcal{X}_1 \times \dots \times \mathcal{X}_Q$, \mathcal{X}_q is the domain of the q^{th} covariate, and Q is the number of covariates. For example in Electronic Health Record (EHR) data, covariate information can include patient information such as age, sex, weight, time since remission, etc. Collectively, instance-specific samples and covariates form the full longitudinal data matrix $Y = [Y_1^T, \dots, Y_P^T]^T = [\mathbf{y}_1, \dots, \mathbf{y}_N]^T$ and covariate matrix $X = [X_1^T, \dots, X_P^T]^T = [\mathbf{x}_1, \dots, \mathbf{x}_N]^T$, respectively. Following the standard notation in generative modelling literature, we denote the low-dimensional latent space of dimensionality L as $\mathcal{Z} = \mathbb{R}^L$ and a latent embedding for all N samples as $Z = [\mathbf{z}_1, \dots, \mathbf{z}_N]^T \in \mathbb{R}^{N \times L}$. We also index Z across L dimensions as $Z = [\tilde{\mathbf{z}}_1, \dots, \tilde{\mathbf{z}}_L]$, where $\tilde{\mathbf{z}}_l = [z_{1l}, \dots, z_{Nl}]^T$ is a vector that contains the l^{th} dimension of the latent embedding across all N samples.

Auto-encoding variational Bayes Consider the joint generative model $p_\omega(\mathbf{y}, \mathbf{z}) = p_\psi(\mathbf{y}|\mathbf{z})p_\theta(\mathbf{z})$ parameterised by $\omega = \{\psi, \theta\}$, and assume we are interested to infer the latent variable \mathbf{z} given \mathbf{y} . The posterior distribution $p_\omega(\mathbf{z}|\mathbf{y}) = p_\psi(\mathbf{y}|\mathbf{z})p_\theta(\mathbf{z})/p_\omega(\mathbf{y})$ is generally intractable due to the marginalisation over the latent space $p_\omega(\mathbf{y}) = \int p_\psi(\mathbf{y}|\mathbf{z})p_\theta(\mathbf{z})d\mathbf{z}$. Auto-Encoding Variational Bayes (AEVB) (Kingma and Welling, 2013) is a powerful deep learning technique for latent variable models that factorise across samples as $p_\omega(Y, Z) = p_\psi(Y|Z)p_\theta(Z) = \prod_{n=1}^N p_\psi(\mathbf{y}_n|\mathbf{z}_n)p_\theta(\mathbf{z}_n)$. AEVB introduces an inference model (also called probabilistic encoder) $q_\phi(\mathbf{z}|\mathbf{y})$, parameterised by ϕ , that seeks to approximate the true posterior. The most well-known AEVB model is the variational autoencoder (VAE), where the inference model as well as the probabilistic decoder $p_\psi(\mathbf{y}|\mathbf{z})$ are parameterised by DNNs. Instead of optimising sample-specific variational parameters, as in standard variational inference (VI), AEVB uses amortised VI that exploits the inference model $q_\phi(\mathbf{z}|\mathbf{y})$ to obtain approximate distributions for each \mathbf{z}_n as a function of the corresponding sample \mathbf{y}_n . Then the approximate inference problem is fitted by maximising the evidence lower bound (ELBO) of the marginal log-likelihood:

$$\log p_\omega(Y) \geq \mathcal{L}(\phi, \psi, \theta; Y) \triangleq \mathbb{E}_{q_\phi(Z|Y)}[\log p_\psi(Y|Z)] - D_{\text{KL}}(q_\phi(Z|Y)||p_\theta(Z)) \longrightarrow \max_{\phi}, \quad (1)$$

where D_{KL} denotes the KL divergence. In practice, the approximate inference is typically conducted simultaneously alongside learning the generative model's parameters via solving the joint optimisation problem $\mathcal{L}(\phi, \psi, \theta; Y) \longrightarrow \max_{\phi, \psi, \theta}$.

2.1 Longitudinal variational autoencoder

The standard VAE model assumes that the joint distribution factorises across samples. Therefore, it can neither capture the potentially non-trivial structure of the data across the samples nor exploit that structure while making predictions. GP-VAE (Fortuin et al., 2019) addresses this issue for multivariate time-series data with a time-dependent GP prior on Z , primarily to address the imputation of missing values. GPPVAE (Casale et al., 2018) targeted the modelling of a time-series of images and extended the VAE with a GP prior whose covariance matrix is factorised into feature and view components.

Building upon the work of Casale et al. (2018) and Fortuin et al. (2019), we propose to enhance the ability of VAEs to learn meaningful low-dimensional representations of Y , with a non-i.i.d. model for the low-dimensional latent space. This would enable our proposed method to effectively capture the structure of the data across the observed samples w.r.t. the auxiliary information X . Specifically, our generative model, parameterised by $\omega = \{\psi, \theta\}$, is formulated as

$$p_\omega(Y|X) = \int_Z p_\psi(Y|Z, X)p_\theta(Z|X)dZ = \int_Z \prod_{n=1}^N p_\psi(\mathbf{y}_n|\mathbf{z}_n)p_\theta(Z|X)dZ, \quad (2)$$

where the probabilistic decoder for normally distributed data,

$$p_\psi(\mathbf{y}_n|\mathbf{z}_n) = \mathcal{N}(\mathbf{y}_n|\mathbf{g}_\psi(\mathbf{z}_n), \text{diag}(\sigma_{y_1}^2, \dots, \sigma_{y_D}^2)) \quad (3)$$

is parameterised by a neural network ψ (variance parameters $\sigma_{y_d}^2$ are included in ψ) and $p_\theta(Z|X)$ is defined by a multi-output GP prior that regulates the joint structure of Z with auxiliary variables X .

2.1.1 Multi-output additive Gaussian process prior

Consider a multi-output function $\mathbf{f} : \mathcal{X} \rightarrow \mathcal{Z} = \mathbb{R}^L$ where $L > 1$, denoted as $\mathbf{f}(\mathbf{x}) = [f_1(\mathbf{x}), \dots, f_L(\mathbf{x})]^T$. Following Alvarez et al. (2011), we denote that \mathbf{f} follows a multi-output Gaussian process prior as $\mathbf{f}(\mathbf{x}) \sim GP(\boldsymbol{\mu}(\mathbf{x}), \mathbf{K}(\mathbf{x}, \mathbf{x}'|\theta))$, where $\boldsymbol{\mu}(\mathbf{x}) \in \mathbb{R}^L$ is the mean (which we assume as $\mathbf{0}$) and $\mathbf{K}(\mathbf{x}, \mathbf{x}'|\theta)$ is a matrix-valued positive definite cross-covariance function (CF) whose entries define the covariances between the output dimensions for any \mathbf{x}, \mathbf{x}' . For any finite collection of inputs $X = [\mathbf{x}_1^T, \dots, \mathbf{x}_N^T]^T$, the corresponding function values $\mathbf{f}(X) = [\mathbf{f}(\mathbf{x}_1)^T, \dots, \mathbf{f}(\mathbf{x}_N)^T]^T \in \mathbb{R}^{NL \times 1}$ have a joint multivariate Gaussian distribution $p(\mathbf{f}(X)) = \mathcal{N}(\mathbf{0}, \mathbf{K}_{XX}(\theta))$, where the covariance matrix $\mathbf{K}_{XX}(\theta)$ is a block-partitioned matrix of size $NL \times NL$ with $L \times L$ blocks, $[\mathbf{K}_{XX}(\theta)]_{i,j} = \mathbf{K}(\mathbf{x}_i, \mathbf{x}_j|\theta)$.

In light of the existing literature, which features a wide range of covariance functions, we make some assumptions for our generative model. First, we consider CFs that factorise across the output dimensions, which is equivalent to $\mathbf{K}(\mathbf{x}, \mathbf{x}'|\theta)$ being diagonal

$$\mathbf{K}(\mathbf{x}, \mathbf{x}'|\theta) = \text{diag}(k_1(\mathbf{x}, \mathbf{x}'|\theta_1), \dots, k_L(\mathbf{x}, \mathbf{x}'|\theta_L)), \quad (4)$$

where $k_l(\mathbf{x}, \mathbf{x}'|\theta_l) = \text{cov}(f_l(\mathbf{x}), f_l(\mathbf{x}'))$ is the CF for the l^{th} latent dimension. We exploit this property to derive an efficient inference algorithm, which we elucidate in section 2.2. Second, we will assume an additive structure for the CF, where each component depends on only a single covariate or a pair of covariates. Such a CF would naturally provide a way to handle heterogeneous inputs, interpretability, and disentanglement for different covariates. Specifically, we assume that

$$\mathbf{f}(\mathbf{x}) = \mathbf{f}^{(1)}(\mathbf{x}^{(1)}) + \dots + \mathbf{f}^{(R)}(\mathbf{x}^{(R)}), \quad \mathbf{f}^{(r)}(\mathbf{x}^{(r)}) \sim GP(\mathbf{0}, \mathbf{K}^{(r)}(\mathbf{x}^{(r)}, \mathbf{x}^{(r)'}|\theta^{(r)})), \quad (5)$$

where each $\mathbf{f}^{(r)}(\mathbf{x}^{(r)})$ is a separate GP with specific parameters $\theta^{(r)}$, and $\mathbf{x}^{(r)} \in \mathcal{X}^{(r)} \subseteq \mathcal{X}$. The covariance function of the additive GP is a sum of its components' covariances $\mathbf{f}(\mathbf{x}) \sim GP(\mathbf{0}, \sum_{r=1}^R \mathbf{K}^{(r)}(\mathbf{x}^{(r)}, \mathbf{x}^{(r)'}|\theta^{(r)}))$ (Williams and Rasmussen, 2006). Furthermore, assuming the multi-variate latent embedding $Z = [\mathbf{z}_1^T, \dots, \mathbf{z}_N^T]^T \in \mathbb{R}^{N \times L}$ is perturbed by i.i.d. zero-mean Gaussian noise with dimension-specific noise variances $\boldsymbol{\sigma}^2 = [\sigma_{z_1}^2, \dots, \sigma_{z_L}^2]$, the GP marginalised likelihood can be obtained as (for notational brevity, variance parameters $\boldsymbol{\sigma}^2$ are included in θ)

$$p_\theta(Z|X) = p(\text{vec}(Z)|X, \theta) = \mathcal{N}\left(\text{vec}(Z)|\mathbf{0}, \sum_{r=1}^R \mathbf{K}_{XX}^{(r)}(\theta^{(r)}) + I_N \otimes \text{diag}(\boldsymbol{\sigma}^2)\right), \quad (6)$$

where $\text{vec}(Z) = [\mathbf{z}_1^T, \dots, \mathbf{z}_N^T]^T$. Given that we assume factorisable CFs, (6) can be written as

$$p(\text{vec}(Z)|X, \theta) = \prod_{l=1}^L p(\bar{\mathbf{z}}_l|X, \theta_l, \sigma_l^2) = \prod_{l=1}^L \mathcal{N}\left(\bar{\mathbf{z}}_l|\mathbf{0}, \sum_{r=1}^R K_{XX}^{(l,r)}(\theta_l^{(r)}) + \sigma_{z_l}^2 I_N\right), \quad (7)$$

where $K_{XX}^{(l,r)}(\theta_l^{(r)})$ is a $N \times N$ covariance matrix for the r^{th} component of the l^{th} latent dimension.

Similar to Cheng et al. (2019), we use the following elementary covariance functions to construct the additive GP components within our framework. Effects of continuous covariates are modelled with the squared exponential CF. Categorical covariates are modelled either alone with the categorical CF or together with the time (or other continuous) covariate using an interaction CF, which is the product of the categorical and squared exponential CFs. The product of the squared exponential CF and the binary CF is used to model covariates that are defined for a subset of samples. An example of such a covariate in a biomedical context is the time to the disease onset, which is defined only for those individuals who get a disease. All CFs for different latent dimensions and additive components have separate parameters $\theta_l^{(r)}$ (LR in total). A detailed description of the CFs is included in the Suppl. Material. Moreover, by restraining to this family of CFs, we are able to devise accurate approximate computational strategies to overcome the typically cubic scaling of GPs as described in section 2.2. Moreover, each additive component has an output scale parameter (or output variance) which is a scale factor that is learnt alongside the other parameters. We constrain the scale parameters to positive values and fix the likelihood noise $\sigma_{z_l}^2$ to 1. In practice, covariates may also comprise of missing values. To handle missingness in the covariates, we set a CF $\mathbf{K}^{(r)}(\mathbf{x}^{(r)}, \mathbf{x}^{(r)'}|\theta^{(r)}) \doteq \mathbf{0}_{L \times L}$ for those sample pairs \mathbf{x} and \mathbf{x}' that contain at least one missing value for the respective covariate(s) in $\mathcal{X}^{(r)}$. This ensures that the contribution of the missing values to the target variable is 0.

2.1.2 Auto-Encoding Variational Bayes for L-VAE

We approximate the true posterior of Z with the product of multivariate Gaussian distributions across samples, each of which has a diagonal covariance matrix:

$$q_\phi(Z|Y) = \prod_{n=1}^N \mathcal{N}(z_n | \mu_\phi(\mathbf{y}_n), \text{diag}(\sigma_\phi^2(\mathbf{y}_n))) = \prod_{n=1}^N \prod_{l=1}^L \mathcal{N}(z_{nl} | \mu_{\phi,l}(\mathbf{y}_n), \sigma_{\phi,l}^2(\mathbf{y}_n)). \quad (8)$$

Here, the probabilistic encoder is represented by neural network functions parameterised by ϕ , $\mu_\phi : \mathbb{R}^D \rightarrow \mathbb{R}^L$ and $\sigma_\phi^2 : \mathbb{R}^D \rightarrow \mathbb{R}_+^L$, that determine the means and variances of the approximating variational distribution. Following the AEVB approach of Kingma and Welling (2013), we form the ELBO for the L-VAE:

$$\log p_\omega(Y|X) \geq \mathcal{L}(\phi, \psi, \theta; Y, X) \triangleq \mathbb{E}_{q_\phi(Z|Y)} [\log p_\psi(Y|Z)] - D_{\text{KL}}(q_\phi(Z|Y) || p_\theta(Z|X)). \quad (9)$$

From equations (2-3) and (8) which describe the factorised decoder and variational approximation respectively, the reconstruction term of the ELBO in eq. (9) consists of additive terms across the samples and observations which can be written as $\mathbb{E}_{q_\phi(Z|Y)} [\log p_\psi(Y|Z)] = \sum_{n=1}^N \sum_{d=1}^D \mathbb{E}_{q_\phi(z_n|\mathbf{y}_n)} [\log p_\psi(y_{nd}|z_n)]$. If Y contains missing values, this summation is done only over the non-missing elements.

Given that our multi-output additive GP prior builds upon CFs that factorise across the latent dimensions $p_\theta(Z|X) = \prod_{l=1}^L p(\bar{z}_l|X, \theta_l, \sigma_{z_l}^2)$, we can exploit the additive nature of the KL divergence for pairs of independent distributions:

$$D_{\text{KL}}(q_\phi(Z|Y, X) || p_\theta(Z|X)) = \sum_{l=1}^L D_{\text{KL}}(q_\phi(\bar{z}_l|Y, X) || p_\theta(\bar{z}_l|X)). \quad (10)$$

Hence, we implicitly avoid dealing with multi-output GPs during model training and can leverage the simplicity as well as efficiency of univariate GPs.

2.2 Efficient KL divergence computation

Optimising the variational objective in eq. (9) involves the computation of the KL divergence in eq. (10), which decomposes into L KL divergences,

$$D_{\text{KL}}^{(l)} = D_{\text{KL}}(q_\phi(\bar{z}_l|Y, X) || p_\theta(\bar{z}_l|X)) = D_{\text{KL}}(\mathcal{N}(\bar{\mu}_l, W_l) || \mathcal{N}(\mathbf{0}, \Sigma_l)), \quad (11)$$

where $\bar{\mu}_l = [\mu_{\phi,l}(\mathbf{y}_1), \dots, \mu_{\phi,l}(\mathbf{y}_N)]^T$, $W_l = \text{diag}(\sigma_{\phi,l}^2(\mathbf{y}_1), \dots, \sigma_{\phi,l}^2(\mathbf{y}_N))$, and $\Sigma_l = \sum_{r=1}^R K_{XX}^{(l,r)} + \sigma_{z_l}^2 I_N$. Each of the KL divergences is available in closed form, but its exact computation requires $\mathcal{O}(N^3)$ flops, which makes it impractical when N exceeds a few thousands. Due to the structured correlation between all the latent samples introduced by the multi-output additive GP prior, we do not use mini-batch based stochastic gradient optimisation for the ELBO as a mini-batch would be inefficient in capturing the correlations. Instead, we introduce a novel strategy to approximately compute this KL divergence for the full data at a significantly reduced computational cost. Without a loss of generality, we drop the index l for the remainder of this section.

A closely related problem has been studied by Titsias (2009) who proposed the well-known free-form variational lower bound for a GP marginal log-likelihood $\log \mathcal{N}(\bar{z}|\mathbf{0}, \Sigma)$, assuming a set of M inducing locations $S = [\mathbf{s}_1, \dots, \mathbf{s}_M]$ in \mathcal{X} and inducing function values $\mathbf{u} = [f(\mathbf{s}_1), \dots, f(\mathbf{s}_M)]^T = [u_1, \dots, u_M]^T$. The free-form bound is known to be tight when M is sufficiently high and the covariance function is smooth enough. However, longitudinal studies, by definition, always contain a categorical covariate corresponding to instances, which makes the covariance function non-continuous. By separating the additive component that corresponds to the interaction between instances and time (or age) from the other additive components, the covariance matrix has the following general form $\Sigma = K_{XX}^{(A)} + \hat{\Sigma}$, where $\hat{\Sigma} = \text{diag}(\hat{\Sigma}_1, \dots, \hat{\Sigma}_P)$, $\hat{\Sigma}_p = K_{X_p X_p}^{(R)} + \sigma_z^2 I_{n_p}$ and $K_{XX}^{(A)} = \sum_{r=1}^{R-1} K_{XX}^{(r)}$ contains all the other $R-1$ components. It is now clear that the exploitation of the free-form bound would mandate that $M \geq P$, thus rendering the bound of Titsias (2009) either computationally inefficient once P is large (due to high M) or insufficiently tight. Since the interaction CF is essential

for accurate longitudinal modelling, we devised a novel free-form divergence upper bound for such a class of GPs:

$$D_{\text{KL}} \leq \frac{1}{2} \left(\text{tr}(\bar{\Sigma}^{-1}W) + \bar{\mu}^T \bar{\Sigma}^{-1} \bar{\mu} - N + \log |\bar{\Sigma}| - \log |W| + \sum_{p=1}^P \text{tr} \left(\hat{\Sigma}_p^{-1} \tilde{K}_{X_p X_p}^{(A)} \right) \right) \quad (12)$$

where $\bar{\Sigma} = K_{XS}^{(A)} K_{SS}^{(A)-1} K_{SX}^{(A)} + \hat{\Sigma}$ and $\tilde{K}_{X_p X_p}^{(A)} = K_{X_p X_p}^{(A)} - K_{X_p S}^{(A)} K_{SS}^{(A)-1} K_{SX_p}^{(A)}$. The computational complexity of such a bound is $\mathcal{O}(\sum_{p=1}^P n_p^3 + NM^2)$ flops, which leads to an approximately similar computational complexity as Titsias (2009) bound when $n_p \simeq M \ll N$, but is significantly tighter. We provide a detailed derivation of this bound in the Suppl. Material.

2.3 Predictive distribution

Given the training samples Y , covariate information X , and learnt parameters ϕ, ψ, θ , the predictive distribution for the high-dimensional out-of-sample data \mathbf{y}_* given covariates \mathbf{x}_* follows

$$\begin{aligned} p_{\omega}(\mathbf{y}_* | \mathbf{x}_*, Y, X) &\approx \int_{\mathbf{z}_*, Z} \underbrace{p_{\psi}(\mathbf{y}_* | \mathbf{z}_*)}_{\text{decode GP prediction}} \underbrace{p_{\theta}(\mathbf{z}_* | \mathbf{x}_*, Z, X)}_{\text{GP predictive posterior}} \underbrace{q_{\phi}(Z | Y, X)}_{\text{encode training samples}} d\mathbf{z}_* dZ = \\ &= \int_{\mathbf{z}_*} \prod_{d=1}^D \mathcal{N}(y_{*d} | g_{\psi,d}(\mathbf{z}_*), \sigma_{y_d}^2) \prod_{l=1}^L \mathcal{N}(z_{*l} | \mu_{*l}, \sigma_{*l}^2) d\mathbf{z}_* \end{aligned} \quad (13)$$

where the means of the predictive low-dimensional representation are $\mu_{*l} = K_{\mathbf{x}_* X}^{(l)} \Sigma_l^{-1} \bar{\mu}_l$ and variances are $\sigma_{*l}^2 = k_{\mathbf{x}_* \mathbf{x}_*}^{(l)} - K_{\mathbf{x}_* X}^{(l)} \Sigma_l^{-1} K_{X \mathbf{x}_*}^{(l)} + K_{\mathbf{x}_* X}^{(l)} \Sigma_l^{-1} W_l \Sigma_l^{-1} K_{X \mathbf{x}_*}^{(l)} + \sigma_{z_l}^2$. See Suppl. Material for more details.

3 Experiments

We demonstrate the efficacy of our method in capturing the underlying data distribution and learning meaningful latent representations, quantifying performance in missing value imputation, reconstructions from the latent space, and by long-term predictions for synthetic images and a real-world medical time series dataset. We compare the performance of our method with various state-of-the-art methods for the respective datasets. Moreover, we have used similar encoder and decoder network architectures when performing comparisons across methods (see Suppl. Material). Additional results showing the latent embeddings, optimisation trajectories, and more comparisons can be found in the Suppl. Material.

In all our experiments, the *id* covariate is used as an identifier of an instance (e.g. patient or unique handwritten digit style) that takes values in $\{1, \dots, P\}$, whereas other covariates are specific for each dataset (e.g. image rotation *angle* or time relative to disease onset *diseaseAge*). For brevity, we denote the additive components with different covariance functions (CFs) as follows: SE CF $\mathbf{f}_{\text{se}}(\cdot)$, categorical CF $\mathbf{f}_{\text{ca}}(\cdot)$, binary CF $\mathbf{f}_{\text{bi}}(\cdot)$, and their interaction CFs $\mathbf{f}_{\text{ca} \times \text{se}}(\cdot \times \cdot)$ and $\mathbf{f}_{\text{bi} \times \text{se}}(\cdot \times \cdot)$.

Rotated MNIST digits We demonstrate our method on a variant of the MNIST dataset that comprises of 400 unique instances of the digit ‘3’ as proposed in Casale et al. (2018). Each instance is rotated through 16 evenly separated rotation angles in $[0, 2\pi)$. That is, we have two covariates: categorical *id* and continues *angle*. As proposed in Casale et al. (2018), we created the test set (out-of-sample predictions) by completely removing one of the rotation angles for each instance and further removed four randomly selected angles to simulate incomplete data. Hence, for each sequence, 5 images are not observed (see fig. 2(a)). Therefore, in this experiment the training set parameters are $P = 400$, $N = 4400$ (where each $n_p = 11$), and $Q = 2$. The test set comprises of 400 test images of one rotation angle each.

Fig. 2(a) demonstrates that our model was able to reconstruct arbitrary rotation angles, including the out-of-sample rotation (fig. 2(b)). Fig. 2(c) compares the mean squared error (MSE) of the test set reconstructions from our method (four different GP variants) and GPPVAE (Casale et al., 2018). The reconstruction loss decreases with increasing latent space dimension L , but our method consistently outperforms the GPPVAE.

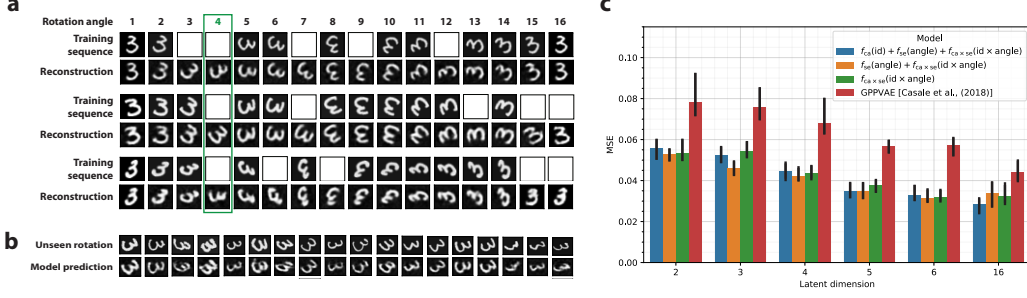


Figure 2: The rotated MNIST experiments. **(a)** Reconstructions obtained from our model using $f_{ca}(id) + f_{se}(angle) + f_{ca \times se}(id \times angle)$, and 16 latent dimensions. The blank boxes corresponds to the missing images. Rotation angle 4 is completely withheld from all instances. **(b)** Predictions for 18 random draws of the out-of-sample prediction state (i.e. unobserved angle in panel **a**). The first row is the real data and the bottom row is our model’s prediction. **(c)** MSE on test set. The error bars represent the minimum and maximum values after 10 repetitions.

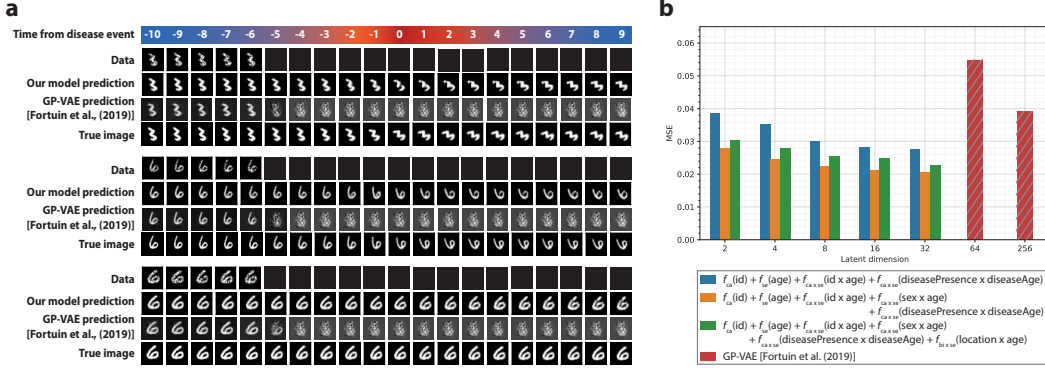


Figure 3: The Health MNIST experiments. **(a)** Reconstructions and predictions obtained from our model using $f_{ca}(id) + f_{se}(age) + f_{ca \times se}(id \times age) + f_{ca \times se}(sex \times age) + f_{ca \times se}(diseasePresence \times diseaseAge)$, and 32 latent dimensions. For GP-VAE, 256 latent dimensions were used. **(b)** MSE from imputing the missing values for observed time points. 3 model variants are shown for L-VAE.

Health MNIST We simulate a longitudinal dataset with missing values using a modified version of the MNIST dataset. The dataset imitates many properties that may be found in actual medical data. In this experiment, we took the digits ‘3’ as well as ‘6’ and assumed that the different digits would represent two biological sexes. To simulate a shared age-related effect, all digit instances were shifted towards the right corner over time. We assume that half of the instances of ‘3’ and ‘6’ remain healthy ($diseasePresence = 0$) and half get a disease ($diseasePresence = 1$). For the diseased instances, we performed a sequence of 20 rotations with the amount of rotation depending on the time to disease diagnosis ($diseaseAge$). We also introduced an irrelevant binary covariate, *location* which is set randomly for each unique instance. To every data point, we applied a random rotational jitter to mimic the addition of noise. We also randomly selected 25% of each image’s pixels and set them as missing — we use these pixels to assess the imputation capability. Therefore, the simulated dataset comprises of $P = 200$ unique instances with a total of $N = 4000$ samples such that each $n_p = 20$. Each sample has $Q = 6$ covariates, namely *age*, *id*, *diseasePresence*, *diseaseAge*, *sex*, and *location*. Additionally, the dataset contained 40 additional instances for which the images of only the first 5 time points are given (as in the ‘Data’ row of fig. 3(a)) — we use these to assess prediction capability. As in Fortuin et al. (2019), we try to draw an analogy to healthcare by assuming that each frame of the time series represents a collection of measurements pertaining to a patient’s health state and that the temporal evolution represents the non-linear evolution of that patient’s health state.

Fig. 3(a) indicates that our approach performs well in reconstructing the temporal trajectory (or disease trajectory as per our analogy) and is able to predict the remaining trajectory, given the corresponding

covariates. The benefits of using our model can especially be seen in the time period $[-4, 9]$ as it effectively captures the non-linear transformation about the disease event. GP-VAE is also capable to effectively reconstruct in the time period $[-10, -6]$, but fails completely in future predictions because it can only utilise the *age* covariate. Fig. 3(b) shows that our model also outperforms GP-VAE (Fortuin et al., 2019) in imputing the missing values for observed time points. Our results indicate that the irrelevant covariate, *location*, has a very mild detrimental effect on the overall model performance. This highlights the robustness of our approach to irrelevant covariates. See Suppl. Fig. 3 and 4 for latent space visualisations.

Healthcare data We evaluated our model on health-care data from the Physionet Challenge 2012 (Silva et al., 2012). The objective of this challenge was to predict the in-hospital mortality of the patients that were monitored in the Intensive Care Unit (ICU) over a period of 48 hours. Similar to Fortuin et al. (2019), we made use of data from 3997 individuals (‘set a’) for training and 3993 individuals for testing (‘set b’). As in Cao et al. (2018), we focused on modelling the measurements of 35 different attributes (such as glucose level, blood pressure, body temperature, etc.), approx. 80% of which are missing in the data. We also made use of 7 patient-specific general auxiliary covariates that were made available as a part of the challenge, i.e. patient identifier (*id*), type of ICU unit (*ICUtype*), *height*, *weight*, *age*, *sex*, in-hospital death (*mortality*) as well as measurement hour (*time*), some of which were also missing for some patients. We constructed an additional covariate (time to mortality or *mortalityTime*) based on the provided survival time. See Suppl. Material for data pre-processing. For model training, data for all patients ($P = 3997$) is available hourly ($n_p = 48$), so $N = 191856$.

We trained our L-VAE model using the training samples and used the fitted deep generative model to build a Bayes classifier aimed at predicting the patient *mortality* for test data. Since the test data lacks information on *mortality* and *mortalityTime* covariates, for each patient in the test set, characterised by a pair of 48 hour attributes time-series Y_* and incomplete auxiliary information X_* , we approximated the marginal log-likelihoods from eq. (9) of the two alternative hypotheses: $L_i = \mathcal{L}(\phi, \psi, \theta; Y_*, X_*, \text{mortality} = i)$ for $i = \{0, 1\}$. Then the predicted mortality probability was computed as $P_1 = \exp(L_1) / (\exp(L_0) + \exp(L_1))$. We provide a detailed explanation of the Bayes classifier and mortality probability P_1 in the Suppl. Material.

To demonstrate the efficacy of our method, we compared the AUROC scores for predicting mortality of the test data instances obtained using our method with those obtained from GP-VAE (Fortuin et al., 2019), HI-VAE (Nazabal et al., 2018), and a standard VAE (Kingma and Welling, 2013). These methods either do not use any auxiliary information (HI-VAE and VAE) or use only the time covariate (GP-VAE). The mortality classification procedure of these methods first imputes the missing values with the generative model, and then exploits the imputed values as covariates to train a logistic regression that is finally used for mortality prediction (Fortuin et al., 2019). Fig. 4 indicates that our L-VAE approach achieves higher AUROC scores. The performance with other additive GP covariance functions can be seen in the Suppl. Material. We trained each model 10 times to assess the stochasticity in performance. In Fortuin et al. (2019), GP-VAE was shown to compare favourably against several other relevant methods, including BRITS (Cao et al., 2018), GRUI-GAN (Luo et al., 2018), and forward/mean imputation (Little and Rubin, 2002), thus strengthening the significance of our results.

4 Discussion

In this paper, we introduced a novel deep generative model, L-VAE, that incorporates auxiliary covariate information to model the structured latent space dynamics for longitudinal datasets with

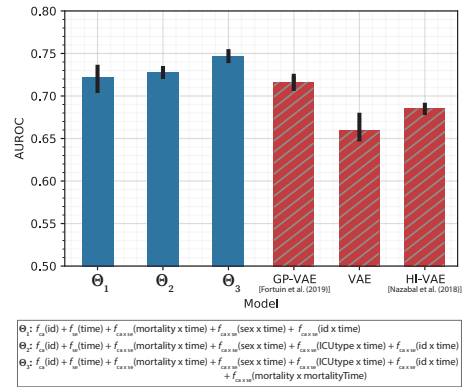


Figure 4: Test set AUROC scores for the patient mortality prediction task for the Physionet Challenge 2012 dataset. The number of latent dimensions is 32. Higher AUROC score is better.

Source code will be made available upon publication.

missing values. We demonstrated the efficacy of our method on synthetic as well as real-world datasets by showing that L-VAE achieves better out-of-sample prediction performance and missing value imputation than competing methods. Moreover, we also introduced a novel computationally efficient inference strategy that exploits the structure of the additive GP covariance functions. Given the flexibility of our model and the state-of-the-art results, we expect L-VAE to become a useful tool for high-dimensional longitudinal data analysis.

For future research, we suggest incorporating a framework for handling heterogeneous data through different likelihood models as proposed in (Nazabal et al., 2018). Our current method holds all data in memory, but we can change our approach to low-memory stochastic gradient approaches that allow scaling the model to even larger datasets.

Broader Impact

Longitudinal data are omnipresent in medicine, finance, meteorology and elsewhere, providing vital information of temporal evolution of the subject of interest, from understanding and predicting a patient’s disease progression to predicting consumer behaviour. For example, clinical time-series are characteristically multivariate, high-dimensional, incomplete in terms of missing values, involve time-varying covariates, and are sampled at irregular time intervals. Although not always appreciated, datasets collected in numerous applications have characteristics that are similar to those of clinical longitudinal datasets. Our proposed deep generative model attempts to learn the data distribution function for the longitudinal data, opening new avenues for in-depth analysis and providing a deeper understanding of the underlying mechanisms of a dataset. Specifically, our L-VAE method incorporates the flexibility of multi-output additive GPs, that allows users to focus on modelling by choosing flexible GP components for their applications, that can account for various types of shared and random effects, the latter being the key defining aspect of longitudinal data. We believe that our proposed method, L-VAE, is very widely applicable to a wide range of applications and brings the commonly used longitudinal modelling concepts into the popular deep learning based VAE framework, thereby opening new research directions for the deep learning community.

We believe that our method does not have any ethical concerns. Failures of our model have the same consequences as failures of any other model if used in an application where reliability is critical, such as in medical and clinical applications. Thus, sufficient testing and validation on independent data is critical to ensure that the training of deep networks has succeeded. Our method is not designed from a privacy preserving stand point (although that would be an interesting future direction, and some previous work in privacy preserving autoencoders (Malekzadeh et al., 2017; Phan et al., 2016) already exists). Therefore, the public release of the L-VAE model that has been trained with sensitive data must be treated confidentially, as with all other non-privacy-preserving methods.

Acknowledgments

This work utilises the computational resources provided by the Aalto Science-IT project. We would like to thank Charles Gadd for the helpful discussions.

References

- S. K. Ainsworth, N. J. Foti, and E. B. Fox. Disentangled VAE representations for multi-aspect and missing data. *arXiv preprint arXiv:1806.09060*, 2018a.
- S. K. Ainsworth, N. J. Foti, A. K. Lee, and E. B. Fox. oi-VAE: Output interpretable VAEs for nonlinear group factor analysis. In *International Conference on Machine Learning*, pages 119–128, 2018b.
- M. A. Alvarez, L. Rosasco, and N. D. Lawrence. Kernels for vector-valued functions: A review. *arXiv preprint arXiv:1106.6251*, 2011.
- W. Cao, D. Wang, J. Li, H. Zhou, L. Li, and Y. Li. BRITS: Bidirectional recurrent imputation for time series. In *Advances in Neural Information Processing Systems*, pages 6775–6785, 2018.
- F. P. Casale, A. Dalca, L. Saglietti, J. Listgarten, and N. Fusi. Gaussian process prior variational autoencoders. In *Advances in Neural Information Processing Systems*, pages 10369–10380, 2018.

- C. Chen, C. Li, L. Chen, W. Wang, Y. Pu, and L. Carin. Continuous-time flows for efficient inference and density estimation. *arXiv preprint arXiv:1709.01179*, 2017.
- L. Cheng, S. Ramchandran, T. Vatanen, N. Lietzén, R. Lahesmaa, A. Vehtari, and H. Lähdesmäki. An additive gaussian process regression model for interpretable non-parametric analysis of longitudinal data. *Nature communications*, 10(1):1–11, 2019.
- L. Dinh, J. Sohl-Dickstein, and S. Bengio. Density estimation using Real NVP. *arXiv preprint arXiv:1605.08803*, 2016.
- V. Fortuin, G. Rätsch, and S. Mandt. GP-VAE: Deep probabilistic time series imputation. *arXiv preprint arXiv:1907.04155*, 2019.
- I. Higgins, L. Matthey, A. Pal, C. Burgess, X. Glorot, M. Botvinick, S. Mohamed, and A. Lerchner. beta-VAE: Learning basic visual concepts with a constrained variational framework. *Iclr*, 2(5):6, 2017.
- D. P. Kingma and M. Welling. Auto-encoding variational bayes. *arXiv preprint arXiv:1312.6114*, 2013.
- T. D. Kulkarni, W. F. Whitney, P. Kohli, and J. Tenenbaum. Deep convolutional inverse graphics network. In *Advances in neural information processing systems*, pages 2539–2547, 2015.
- R. J. Little and D. B. Rubin. Single imputation methods. *Statistical analysis with missing data*, pages 59–74, 2002.
- Y. Luo, X. Cai, Y. Zhang, J. Xu, et al. Multivariate time series imputation with generative adversarial networks. In *Advances in Neural Information Processing Systems*, pages 1596–1607, 2018.
- M. Malekzadeh, R. G. Clegg, and H. Haddadi. Replacement autoencoder: A privacy-preserving algorithm for sensory data analysis. *arXiv preprint arXiv:1710.06564*, 2017.
- K. Mörtens, K. R. Campbell, and C. Yau. Decomposing feature-level variation with covariate gaussian process latent variable models. *arXiv preprint arXiv:1810.06983*, 2018.
- T. Müller, B. McWilliams, F. Rousselle, M. Gross, and J. Novák. Neural importance sampling. *arXiv preprint arXiv:1808.03856*, 2018.
- A. Nazabal, P. M. Olmos, Z. Ghahramani, and I. Valera. Handling incomplete heterogeneous data using vaes. *arXiv preprint arXiv:1807.03653*, 2018.
- N. Phan, Y. Wang, X. Wu, and D. Dou. Differential privacy preservation for deep auto-encoders: an application of human behavior prediction. In *Thirtieth AAAI Conference on Artificial Intelligence*, 2016.
- J. Quiñero-Candela and C. E. Rasmussen. A unifying view of sparse approximate gaussian process regression. *Journal of Machine Learning Research*, 6(Dec):1939–1959, 2005.
- D. J. Rezende and S. Mohamed. Variational inference with normalizing flows. *arXiv preprint arXiv:1505.05770*, 2015.
- I. Silva, G. Moody, D. J. Scott, L. A. Celi, and R. G. Mark. Predicting in-hospital mortality of icu patients: The physionet/computing in cardiology challenge 2012. In *2012 Computing in Cardiology*, pages 245–248. IEEE, 2012.
- K. Sohn, H. Lee, and X. Yan. Learning structured output representation using deep conditional generative models. In *Advances in neural information processing systems*, pages 3483–3491, 2015.
- M. Titsias. Variational learning of inducing variables in sparse gaussian processes. In *Artificial Intelligence and Statistics*, pages 567–574, 2009.
- C. K. Williams and C. E. Rasmussen. *Gaussian processes for machine learning*, volume 2. MIT press Cambridge, MA, 2006.

Longitudinal Variational Autoencoder Supplementary Material

Siddharth Ramchandran¹ Gleb Tikhonov¹ Miika Koskinen^{2,3} Harri Lähdesmäki¹

¹Department of Computer Science, Aalto University, Finland

²Helsinki Biobank, HUS Helsinki University Hospital, Finland

³Faculty of Medicine, University of Helsinki, Finland

{siddharth.ramchandran, gleb.tikhonov, harri.lahdesmaki}@aalto.fi

1 Covariance functions

Squared exponential CF

Let $\mathbf{x}^{(r)} = x \in \mathcal{X}_j$ denote an univariate continuous-valued covariate. The squared exponential (SE) CF is defined as

$$k_{\text{se}}(\mathbf{x}^{(r)}, \mathbf{x}^{(r)'} | \theta_{\text{se}}) = \sigma_{\text{se}}^2 \exp \left(-\frac{(x - x')^2}{2l_{\text{se}}^2} \right), \quad \theta_{\text{se}} = (\sigma_{\text{se}}^2, l_{\text{se}}) \quad (1)$$

where σ_{se}^2 is the magnitude parameter (also called scale) and $l_{\text{se}} \geq 0$ is the length-scale. The magnitude controls the marginal variance of the GP and length-scale controls its smoothness [Williams and Rasmussen, 2006].

Categorical CF

Let $\mathbf{x}^{(r)} = x \in \mathcal{X}_j$ denote a categorical or discrete covariate. Categorical CF is

$$k_{\text{ca}}(\mathbf{x}^{(r)}, \mathbf{x}^{(r)'}) = \begin{cases} 1, & \text{if } x = x' \\ 0, & \text{otherwise} \end{cases} \quad \theta_{\text{ca}} = \emptyset \quad (2)$$

Binary CF

Let $\mathbf{x}^{(r)} = x \in \mathcal{X}_j$ denote an arbitrary univariate covariate. Binary CF is

$$k_{\text{bi}}(\mathbf{x}^{(r)}, \mathbf{x}^{(r)'}) = \begin{cases} 1, & \text{if } x = x' = 1 \\ 0, & \text{otherwise} \end{cases} \quad \theta_{\text{bi}} = \emptyset \quad (3)$$

Interaction CF

Let $\mathbf{x}^{(r)} = [\mathbf{x}^{(a)T}, \mathbf{x}^{(b)T}]^T$, where $\mathbf{x}^{(a)}$ and $\mathbf{x}^{(b)}$ are arbitrary sub-vectors of \mathbf{x} . We define the interaction CF for these subsets as the product of two CFs defined over $\mathbf{x}^{(a)}$ and $\mathbf{x}^{(b)}$ respectively:

$$k_{\text{in}}(\mathbf{x}^{(r)}, \mathbf{x}^{(r)'}) = k^{(a)}(\mathbf{x}^{(a)}, \mathbf{x}^{(a)'}) k^{(b)}(\mathbf{x}^{(b)}, \mathbf{x}^{(b)'}) \quad (4)$$

where $\theta^{(r)} = \theta^{(a)} \cup \theta^{(b)}$. The interaction CF enables us to combine any combination of univariate SE, categorical, and binary CFs in a product CF. However, in practice we restrict such combinations to include no more than a single SE CF. As Cheng et al. [2019] stated, such a condition affords the SE GP flexibility with random intercept/slope constructions similar to the linear mixed effect modelling framework, without sacrificing interpretability. For example, in longitudinal studies an

instance-specific auto-correlated temporal deviation from the population temporal mean can be captured by the interaction term between a categorical CF over the instance identifiers and a SE CF over the temporal covariate. Furthermore, Cheng et al. [2019] adapted an approach to handle missing covariates based on the interaction CF containing a missing-ness mask.

2 Efficient KL divergence computation

As the main text states, optimising the variational objective of L-VAE involves the computation of L KL divergences $D_{\text{KL}} = D_{\text{KL}}(\mathcal{N}(\bar{\mu}_l, W_l) || \mathcal{N}(\mathbf{0}, \Sigma_l))$, where $\bar{\mu}_l = [\mu_{\phi,l}(\mathbf{y}_1), \dots, \mu_{\phi,l}(\mathbf{y}_N)]^T$, $W_l = \text{diag}(\sigma_{\phi,l}^2(\mathbf{y}_1), \dots, \sigma_{\phi,l}^2(\mathbf{y}_N))$, and $\Sigma_l = \sum_{r=1}^R K_{XX}^{(l,r)} + \sigma_z^2 I_N$. In the following, we drop the index l for notational simplicity. Each of the KL divergences is available in closed form using the well-known expression for the KL divergence between two multivariate normal distributions

$$D_{\text{KL}} = \frac{1}{2} (\text{tr}(\Sigma^{-1}W) + \bar{\mu}^T \Sigma^{-1} \bar{\mu} - N + \log |\Sigma| - \log |W|),$$

but its exact computation requires $\mathcal{O}(N^3)$ flops, which makes it impractical when N exceeds a few thousands. In this section, we provide a derivation of a novel strategy to approximately compute this KL divergence at a reduced computational cost.

KL divergence and evidence lower bound We start by exploiting the diagonal structure of W and establish the connection between the upper bound for D_{KL} and the evidence lower bound for the marginal log likelihood (MLL) of a Gaussian process

$$\begin{aligned} D_{\text{KL}}(\mathcal{N}(\bar{\mu}, W) || \mathcal{N}(\mathbf{0}, \Sigma)) &\triangleq \int_{\mathbf{z}} \mathcal{N}(\mathbf{z} | \bar{\mu}, W) \log \left(\frac{\mathcal{N}(\mathbf{z} | \bar{\mu}, W)}{\mathcal{N}(\mathbf{z} | \mathbf{0}, \Sigma)} \right) d\mathbf{z} \\ &= - \int_{\mathbf{z}} \log(\mathcal{N}(\mathbf{z} | \mathbf{0}, \Sigma)) \mathcal{N}(\mathbf{z} | \bar{\mu}, W) d\mathbf{z} - \frac{1}{2} \log |(2\pi e)W| \\ &\leq - \int_{\mathbf{z}} \mathcal{L}(\mathbf{z}; \Sigma) \mathcal{N}(\mathbf{z} | \bar{\mu}, W) d\mathbf{z} - \frac{1}{2} \log |(2\pi e)W| \quad (5) \\ &\text{for any function } \mathcal{L}(\mathbf{z}; \Sigma) : \mathcal{L}(\mathbf{z}; \Sigma) \leq \log(\mathcal{N}(\mathbf{z} | \mathbf{0}, \Sigma)) \quad \forall \mathbf{z} \end{aligned}$$

Hence, for any lower bound of GP MLL $\mathcal{L}(\mathbf{z}; \Sigma)$, the corresponding expression would provide an upper bound for KL divergence between the considered multivariate normal distributions, but lower bound of GP MLL is a much more common and well-studied problem. Please note that in the expression (5) and further throughout this section, we specifically use the lower bound notation for GP MLL lower bound $\mathcal{L}(\mathbf{z}; \Sigma)$, not for the lower bound of the deep generative model as in the main text.

Variational learning of inducing variables in sparse Gaussian processes One of the most fundamental works on ELBOs for GP MLL was conducted by Titsias [2009], and is based on the paradigm of low-rank inducing point approximations of GPs. We briefly recap their key results here, and later build on their derivation to acquire modifications that would suit the structure of matrices Σ in our problem setting.

We denote the set of inducing points locations in \mathcal{X} as $S = [\mathbf{s}_1^T, \dots, \mathbf{s}_M^T]^T$, and the value of the Gaussian process at the inducing locations as $\mathbf{u} = [u_1, \dots, u_M]^T$. We recall that $\Sigma = K_{XX} + \sigma_z^2 I_N$ and therefore, \mathbf{z} can be represented as the sum of noise-free GP $\mathbf{f} \sim \mathcal{N}(\mathbf{0}, K_{XX})$ and i.i.d. Gaussian noise. The following identities always stand

$$p(\mathbf{z} | \mathbf{f}) = \mathcal{N}(\mathbf{z} | \mathbf{f}, \sigma_z^2 I_N) \quad (6)$$

$$p(\mathbf{f} | \mathbf{u}) = \mathcal{N}(\mathbf{f} | K_{XS} K_{SS}^{-1} \mathbf{u}, \tilde{K}), \quad (7)$$

$$\tilde{K} = K_{XX} - K_{XS} K_{SS}^{-1} K_{SX} \quad (8)$$

$$p(\mathbf{u}) = \mathcal{N}(\mathbf{u} | \mathbf{0}, K_{SS}) \quad (9)$$

$$p(\mathbf{z}) = \int_{\mathbf{u}} \int_{\mathbf{f}} p(\mathbf{z} | \mathbf{f}) p(\mathbf{f} | \mathbf{u}) p(\mathbf{u}) d\mathbf{f} d\mathbf{u}. \quad (10)$$

Applying the Jensen inequality on the conditional log-probability $p(\mathbf{z}|\mathbf{u})$ leads to:

$$\log p(\mathbf{z}|\mathbf{u}) = \log \int_{\mathbf{f}} p(\mathbf{z}|\mathbf{f})p(\mathbf{f}|\mathbf{u})d\mathbf{f} \quad (11)$$

$$\geq \int_{\mathbf{f}} \log(p(\mathbf{z}|\mathbf{f}))p(\mathbf{f}|\mathbf{u})d\mathbf{f} = \sum_{i=1}^N \left[\log \mathcal{N}(z_i|\mu_i, \sigma_z^2) - \frac{\tilde{K}_{ii}}{2\sigma_z^2} \right], \quad (12)$$

where $\boldsymbol{\mu} = [\mu_1, \dots, \mu_N]^T = K_{XS}K_{SS}^{-1}\mathbf{u}$ and \tilde{K}_{ii} denotes the i^{th} diagonal element of \tilde{K} . The inequation reduces to identity *iff* the \mathbf{u} is a sufficient statistic of \mathbf{f} . However, the inequation remains tight and the approximation is justified as long as the \tilde{K}_{ii} elements remain small, which is achieved by setting M to be sufficiently high and optimising the inducing points location S . After integrating out the \mathbf{u} , this approximation leads to the collapsed representation of the variational evidence lower bound

$$\mathcal{L}_1(\mathbf{z}; \Sigma) \triangleq \log \mathcal{N}(\mathbf{z}|\mathbf{0}, K_{XS}K_{SS}^{-1}K_{SX} + \sigma_z^2 I_N) - \frac{1}{2\sigma_z^2} \text{tr}(\tilde{K}) \quad (13)$$

Divergence upper bound for longitudinal Gaussian process The free-form bound is known to be tight when M is sufficiently high and the covariance function is smooth enough. However, longitudinal studies, by definition, always contain a categorical covariate corresponding to instances, which makes the covariance function non-continuous. By separating the additive component that corresponds to the interaction between instances and time (or age) from the other additive components, the covariance matrix has the following general form $\Sigma = K_{XX}^{(A)} + \hat{\Sigma}$, where $\hat{\Sigma} = \text{diag}(\hat{\Sigma}_1, \dots, \hat{\Sigma}_P)$, $\hat{\Sigma}_p = K_{X_p X_p}^{(R)} + \sigma_z^2 I_{n_p}$ and $K_{XX}^{(A)} = \sum_{r=1}^{R-1} K_{XX}^{(r)}$ contains all the other $R - 1$ components. In order to keep the \tilde{K}_{ii} tight, the bound from eq. (13) would mandate that $M \geq P$, thus rendering the bound of Titsias [2009] either computationally inefficient once P is large (due to high M) or insufficiently tight. Since the interaction covariance function is essential for accurate longitudinal modelling, we devised a novel free-form divergence upper bound for such a class of GPs. In a similar manner as in eq. (6), we exploit the opportunity to represent \mathbf{z} as a sum of $\mathbf{f}_A \sim \mathcal{N}(\mathbf{0}, K_{XX}^{(A)})$ and $\hat{\mathbf{f}} \sim \mathcal{N}(\mathbf{0}, \hat{\Sigma})$, and we assign the inducing points and values for \mathbf{f}_A . We denote $\tilde{K}^{(A)} = K_{XX}^{(A)} - K_{XS}^{(A)}K_{SS}^{(A)-1}K_{SX}^{(A)}$ and $\tilde{K}_{X_p X_p}^{(A)} = K_{X_p X_p}^{(A)} - K_{X_p S}^{(A)}K_{SS}^{(A)-1}K_{S X_p}^{(A)}$, then

$$\log p(\mathbf{z}|\mathbf{u}) = \log \int_{\mathbf{f}_A} p(\mathbf{z}|\mathbf{f}_A)p(\mathbf{f}_A|\mathbf{u})d\mathbf{f}_A \quad (14)$$

$$= \log \int_{\mathbf{f}_A} \mathcal{N}(\mathbf{z}|\mathbf{f}_A, \hat{\Sigma})\mathcal{N}(\mathbf{f}_A|K_{XS}^{(A)}K_{SS}^{(A)-1}\mathbf{u}, \tilde{K}^{(A)})d\mathbf{f}_A \quad (15)$$

$$\geq \int_{\mathbf{f}_A} \log \left(\mathcal{N}(\mathbf{z}|\mathbf{f}_A, \hat{\Sigma}) \right) \mathcal{N}(\mathbf{f}_A|K_{XS}^{(A)}K_{SS}^{(A)-1}\mathbf{u}, \tilde{K}^{(A)})d\mathbf{f}_A \quad (16)$$

$$= \sum_{p=1}^P \left[\log \mathcal{N}(\mathbf{z}_p|\boldsymbol{\mu}_p, \hat{\Sigma}_p) - \frac{1}{2} \text{tr} \left(\hat{\Sigma}_p^{-1} \tilde{K}_{X_p X_p}^{(A)} \right) \right], \quad (17)$$

where \mathbf{z}_p is the sub-vector of \mathbf{z} that corresponds to the p^{th} individual, $\boldsymbol{\mu}_p$ is the subvector of $K_{XS}^{(A)}K_{SS}^{(A)-1}\mathbf{u}$, and $\text{tr}(\cdot)$ denotes the trace operator. After integrating out the \mathbf{u} , we obtain a novel variational evidence lower bound

$$\mathcal{L}_2(\mathbf{z}; \Sigma) \triangleq \log \mathcal{N}(\mathbf{z}|\mathbf{0}, K_{XS}^{(A)}K_{SS}^{(A)-1}K_{SX}^{(A)} + \hat{\Sigma}) - \frac{1}{2} \sum_{p=1}^P \text{tr} \left(\hat{\Sigma}_p^{-1} \tilde{K}_{X_p X_p}^{(A)} \right). \quad (18)$$

We substitute this lower bound to the expression (5) that links the ELBO and upper bound for KLD:

$$D_{\text{KL}} = D_{\text{KL}}(\mathcal{N}(\bar{\mu}, W) || \mathcal{N}(\mathbf{0}, \Sigma)) \leq - \int_{\mathbf{z}} \mathcal{L}_2(\mathbf{z}; \Sigma) \mathcal{N}(\mathbf{z} | \bar{\mu}, W) d\mathbf{z} - \frac{1}{2} \log |(2\pi e)W| \quad (19)$$

$$= - \int_{\mathbf{z}} \log \mathcal{N} \left(\mathbf{z} | K_{XS}^{(A)} K_{SS}^{(A)-1} K_{SX}^{(A)} + \hat{\Sigma} \right) \mathcal{N}(\mathbf{z} | \bar{\mu}, W) d\mathbf{z} - \frac{1}{2} \log |(2\pi e)W| + \frac{1}{2} \sum_{p=1}^P \text{tr} \left(\hat{\Sigma}_p^{-1} \tilde{K}_{X_p X_p}^{(A)} \right) \quad (20)$$

$$= D_{\text{KL}} \left(\mathcal{N}(\bar{\mu}, W) || \mathcal{N}(\mathbf{0}, K_{XS}^{(A)} K_{SS}^{(A)-1} K_{SX}^{(A)} + \hat{\Sigma}) \right) + \frac{1}{2} \sum_{p=1}^P \text{tr} \left(\hat{\Sigma}_p^{-1} \tilde{K}_{X_p X_p}^{(A)} \right) \quad (21)$$

$$= \frac{1}{2} \left(\text{tr}(\bar{\Sigma}^{-1} W) + \bar{\mu}^T \bar{\Sigma}^{-1} \bar{\mu} - N + \log |\bar{\Sigma}| - \log |W| + \sum_{p=1}^P \text{tr} \left(\hat{\Sigma}_p^{-1} \tilde{K}_{X_p X_p}^{(A)} \right) \right), \quad (22)$$

where $\bar{\Sigma} = K_{XS}^{(A)} K_{SS}^{(A)-1} K_{SX}^{(A)} + \hat{\Sigma}$.

Computational complexity The computational complexity of bound (19) is $\mathcal{O}(\sum_{p=1}^P n_p^3 + NM^2)$ flops, which leads to approximately similar computational complexity as Titsias [2009] bound, when $n_p \simeq M \ll N$, but is significantly tighter. Here, we elucidate in detail how to perform the computations in eq. (19) to achieve such complexity. The first term of (19) can be written as

$$\text{tr}(\bar{\Sigma}^{-1} W) = \text{tr}(\hat{\Sigma}^{-1} W) - \text{tr} \left(\hat{\Sigma}^{-1} K_{XS}^{(A)} \left[K_{SS}^{(A)} + K_{SX}^{(A)} \hat{\Sigma}^{-1} K_{XS}^{(A)} \right]^{-1} K_{SX}^{(A)} \hat{\Sigma}^{-1} W \right) \quad (23)$$

$$= \sum_{p=1}^P \left(\text{diag}(\hat{\Sigma}^{-1}) \cdot \text{diag}(W_p) \right) - \text{tr} \left(H^{-1} \left(K_{SX}^{(A)} \hat{\Sigma}^{-1} W \hat{\Sigma}^{-1} K_{XS}^{(A)} \right) \right), \quad (24)$$

where $H = K_{SS}^{(A)} + K_{SX}^{(A)} \hat{\Sigma}^{-1} K_{XS}^{(A)}$ and we have used the Woodbury matrix identity to obtain the first equality and the cyclic rotation property of the matrix trace to obtain the second equality [Press et al., 2007]. Since $\hat{\Sigma}$ is a block-diagonal matrix, obtaining $\hat{\Sigma}^{-1}$ takes $\mathcal{O}(\sum_{p=1}^P n_p^3)$ flops and obtaining products $K_{SX}^{(A)} \hat{\Sigma}^{-1} K_{XS}^{(A)}$ or $K_{SX}^{(A)} (\hat{\Sigma}^{-1} W \hat{\Sigma}^{-1}) K_{XS}^{(A)}$ takes $\mathcal{O}(\sum_{p=1}^P n_p M^2) = \mathcal{O}(NM^2)$ flops. Inverting H takes $\mathcal{O}(M^3)$ flops.

We can use the Woodbury matrix identity to write the second term as

$$\bar{\mu}^T \bar{\Sigma}^{-1} \bar{\mu} = \bar{\mu}^T \hat{\Sigma}^{-1} \bar{\mu} - \bar{\mu}^T \hat{\Sigma}^{-1} K_{XS}^{(A)} H^{-1} K_{SX}^{(A)} \hat{\Sigma}^{-1} \bar{\mu}.$$

Obtaining $\hat{\Sigma}^{-1} \bar{\mu}$ takes $\mathcal{O}(\sum_{p=1}^P n_p^2)$ flops and obtaining $K_{SX}^{(A)} (\hat{\Sigma}^{-1} \bar{\mu})$ takes $\mathcal{O}(NM^2)$ flops.

For the forth term we use the generalised determinant lemma so that

$$|\bar{\Sigma}| = |\hat{\Sigma}| |K_{SS}^{(A)}|^{-1} |H|.$$

These determinant computations take $\mathcal{O}(\sum_{p=1}^P n_p^3)$, $\mathcal{O}(M^3)$ and $\mathcal{O}(M^3)$, correspondingly.

The fifth term is trivially $\mathcal{O}(N)$, whereas we can again use the cyclic rotation property of the matrix trace to write the last term as

$$\text{tr} \left(\hat{\Sigma}_p^{-1} \tilde{K}_{X_p X_p}^{(A)} \right) = \text{tr} \left(\hat{\Sigma}_p^{-1} K_{X_p X_p}^{(A)} \right) - \text{tr} \left(\hat{\Sigma}_p^{-1} K_{X_p S}^{(A)} K_{SS}^{(A)-1} K_{SX_p}^{(A)} \right) \quad (25)$$

$$= \text{tr} \left(\hat{\Sigma}_p^{-1} K_{X_p X_p}^{(A)} \right) - \text{tr} \left(\left(K_{SX_p}^{(A)} \hat{\Sigma}_p^{-1} K_{X_p S}^{(A)} \right) K_{SS}^{(A)-1} \right). \quad (26)$$

The first trace takes $\mathcal{O}(n_p^2)$ to compute once the $\hat{\Sigma}^{-1}$ is available. It takes $\mathcal{O}(n_p M^2)$ to compute the product in parenthesis in the second trace and $\mathcal{O}(M^2)$ for the trace itself once $K_{SS}^{(A)-1}$ is available. Since we need to compute these traces for $p = 1, \dots, P$, the overall complexity of the last term in eq. (19) is $\mathcal{O}(\sum_{p=1}^P n_p^2 + NM^2)$.

Combining the terms we get the final time complexity

$$\text{Complexity} = \mathcal{O}\left(\sum_{p=1}^P n_p^3\right) + \mathcal{O}(NM^2) + \mathcal{O}(M^3) + \mathcal{O}\left(\sum_{p=1}^P n_p^2\right) + \mathcal{O}(NM^2) \quad (27)$$

$$+ \mathcal{O}\left(\sum_{p=1}^P n_p^3\right) + \mathcal{O}(M^3) + \mathcal{O}(M^3) + \mathcal{O}(N) + \mathcal{O}\left(\sum_{p=1}^P n_p^2 + NM^2\right) \quad (28)$$

$$= \mathcal{O}\left(\sum_{p=1}^P n_p^3 + NM^2\right). \quad (29)$$

3 Predictive distribution

The problem of obtaining the predictive distribution for the high-dimensional out-of-sample data \mathbf{y}_* given covariates \mathbf{x}_* with L-VAE can be split into two parts: obtaining the predictive distribution of the latent representation \mathbf{z}_* and propagating the obtained distribution through the probabilistic decoder $p(\mathbf{y}_*|\mathbf{z}_*)$. Given the training samples Y , covariate information X , as well as learnt parameters of the generative model $\omega = \{\psi, \theta\}$ and the inference model ϕ , the predictive distribution follows

$$p_\omega(\mathbf{y}_*|\mathbf{x}_*, Y, X) = \int_{\mathbf{z}_*} p_\omega(\mathbf{y}_*|\mathbf{z}_*, \mathbf{x}_*, Y, X) p_\omega(\mathbf{z}_*|\mathbf{x}_*, Y, X) d\mathbf{z}_* \quad (30)$$

$$= \int_{\mathbf{z}_*, Z} \underbrace{p_\psi(\mathbf{y}_*|\mathbf{z}_*)}_{\text{decode GP prediction}} \underbrace{p_\theta(\mathbf{z}_*|\mathbf{x}_*, Z, X)}_{\text{GP predictive posterior}} \underbrace{p_\omega(Z|Y, X)}_{\text{posterior of } Z} d\mathbf{z}_* dZ \quad (31)$$

$$\approx \int_{\mathbf{z}_*, Z} \underbrace{p_\psi(\mathbf{y}_*|\mathbf{z}_*)}_{\text{decode GP prediction}} \underbrace{p_\theta(\mathbf{z}_*|\mathbf{x}_*, Z, X)}_{\text{GP predictive posterior}} \underbrace{q_\phi(Z|Y, X)}_{\text{encode training samples}} d\mathbf{z}_* dZ. \quad (32)$$

The true posterior $p_\omega(Z|Y, X)$ is intractable and, similar to the model inference or learning problem, it is replaced with the variational approximation defined by the inference model $q_\phi(Z|Y, X)$. Given such an approximate substitution, the (approximate) predictive GP distribution for the latent representation is available in closed form

$$\hat{p}_\omega(\mathbf{z}_*|\mathbf{x}_*, Y, X) = \int_Z p_\theta(\mathbf{z}_*|\mathbf{x}_*, Z, X) q_\phi(Z|Y, X) dZ = N(\mathbf{z}_*|\boldsymbol{\mu}_*, \Sigma_*). \quad (33)$$

Since in the current work we only consider multi-output GPs with diagonal cross-covariance functions and the output of probabilistic encoder $p_\psi(\mathbf{y}_n|\mathbf{z}_n)$ is restricted to be a multivariate normal distribution with diagonal covariance matrix, the predictive distribution in the latent space also factorises across the latent dimensions $N(\mathbf{z}_*|\boldsymbol{\mu}_*, \Sigma_*) = \prod_{l=1}^L N(z_{*l}|\mu_{*l}, \sigma_{*l}^2)$ with:

$$\mu_{*l} = K_{\mathbf{x}_* X}^{(l)} \Sigma_l^{-1} \bar{\boldsymbol{\mu}}_l \quad (34)$$

$$\sigma_{*l}^2 = k_{\mathbf{x}_* \mathbf{x}_*}^{(l)} - K_{\mathbf{x}_* X}^{(l)} \Sigma_l^{-1} K_{X \mathbf{x}_*}^{(l)} + K_{\mathbf{x}_* X}^{(l)} \Sigma_l^{-1} W_l \Sigma_l^{-1} K_{X \mathbf{x}_*}^{(l)} + \sigma_{zl}^2, \quad (35)$$

where $k_{\mathbf{x}_* \mathbf{x}_*}^{(l)} = K_{\mathbf{x}_* \mathbf{x}_*}^{(l)} = \sum_{r=1}^R K_{\mathbf{x}_* \mathbf{x}_*}^{(l,r)}(\theta_l^{(r)})$ and $K_{\mathbf{x}_* X}^{(l)} = K_{X \mathbf{x}_*}^{(l)T} = \sum_{r=1}^R K_{\mathbf{x}_* X}^{(l,r)}(\theta_l^{(r)})$ (see eq. (8) in the main text), and $\Sigma_l = \sum_{r=1}^R K_{XX}^{(l,r)}(\theta_l^{(r)}) + \sigma_{zl}^2 I$, $W_l = \text{diag}(\sigma_{\phi,l}^2(\mathbf{y}_1), \dots, \sigma_{\phi,l}^2(\mathbf{y}_N))$ and $\bar{\boldsymbol{\mu}}_l = [\mu_{\phi,l}(\mathbf{y}_1), \dots, \mu_{\phi,l}(\mathbf{y}_N)]^T$ (as in eq. (12) in the main text). Incorporating this property with eq. (32) leads to,

$$p_\omega(\mathbf{y}_*|\mathbf{x}_*, Y, X) \approx \int_{\mathbf{z}_*} \prod_{d=1}^D \mathcal{N}(y_{*d} | g_{\psi,d}(\mathbf{z}_*), \sigma_{yd}^2) \prod_{l=1}^L \mathcal{N}(z_{*l} | \mu_{*l}, \sigma_{*l}^2) d\mathbf{z}_*. \quad (36)$$

4 Downstream classification task in the healthcare data experiment

Given the test set, our objective is to predict the patient *mortality*. Since our proposed model is generative in nature, we must include the *mortality* covariate in the additive GP prior. The downstream

classification task is done by computing the probability that $mortality = 0$ and $mortality = 1$. Given the learnt L-VAE model with fixed parameters ϕ, ψ, θ , we can obtain the probability for the binary mortality event for each patient (X_*, Y_*) in the test set as,

$$P(mortality = 0) = \frac{\exp(\mathcal{L}(\phi, \psi, \theta; Y_*, X_*, mortality = 0))}{\sum_{i=0}^1 \exp(\mathcal{L}(\phi, \psi, \theta; Y_*, X_*x, mortality = i))},$$

$$P(mortality = 1) = 1 - P(mortality = 0).$$

Furthermore, we also introduce a time to mortality covariate (or *mortalityTime*) that is based on the survival time. This covariate is relevant for individuals whose $mortality = 1$ and is treated as missing for the individuals that survive. However, in the testing phase, the exact mortality time is not known as we are trying to perform classification based on *mortality*. To overcome this problem, we estimate the distribution of the *mortalityTime* covariate based on the values of the covariate in the training set and, in the test time, we compute the expectation of the ELBO described in eq. (10) of the main manuscript w.r.t. to that distribution. We approximate the expectation with a finite weighted average. Concretely, we first allocate the *mortalityTime* covariate values in the training set into B bins based on a logarithmic scale. Let α_i be the bin count and t_i be the average value of the *mortalityTime* in the i^{th} bin. The proportion of *mortalityTime* values in bin i is $w_i = \alpha_i / (\sum_{i=1}^B \alpha_i)$. The weighted ELBO is then computed as

$$\mathcal{L}(\phi, \psi, \theta; Y, X, mortality = 1) = \sum_{i=1}^B w_i \cdot \mathcal{L}(\phi, \psi, \theta; Y, X, mortality = 1, t_i),$$

where the ELBO terms are now explicitly conditioned by the *mortalityTime* t_i . We use $B = 6$ in our analysis. The histograms of the survival times in the training and test data are shown in fig. 1.

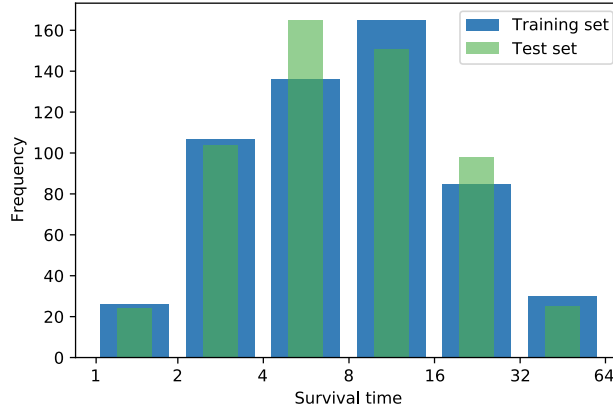


Figure 1: Histogram of survival times in training and test set

5 Optimisation and practical considerations

We make use of a suitable stochastic optimisation technique to minimise the ELBO in eq. (9) of the main manuscript. The parameters that we need to optimise include the neural network weights (ϕ and ψ) and kernel parameters (θ) of the multi-output additive GPs. In particular, the optimisation is done using the Adam optimiser [Kingma and Ba, 2014], which is an adaptive learning rate method that maintains an exponentially decaying average of past gradients as well as squared gradients. For the inference implementation, we make use of PyTorch [Paszke et al., 2019] which allows the computation of derivatives using automatic differentiation.

In all the experiments, we first pre-train the neural networks with a standard normal distribution as the prior on the latent space (standard VAE [Kingma and Welling, 2013]) for 1000 epochs. This is followed by training the L-VAE model using the pre-trained encoder and decoder networks as initial values for ϕ and ψ , respectively. In the Rotated MNIST and Health MNIST experiments, L-VAE is

trained for 2000 epochs. Moreover, in the Healthcare data experiment, L-VAE is trained for 1000 epochs.

6 Supplementary tables

Table 1 describes the neural network architecture used for the Rotated MNIST experiment. The hyperparameter choices are similar to Casale et al. [2018]. The architecture used for the Health MNIST experiment is described in table 2. We have tried to replicate the hyperparameter choices from Fortuin et al. [2019] for this experiment. For the Physionet Challenge 2012 dataset, we did not make use of a convolutional neural network (CNN) as was done for the Rotated MNIST as well Health MNIST experiments because CNNs are more appropriate for image based (visual) data where the regional correlation (receptive field) of the measured values is important [Goodfellow et al., 2016]. Table 3 describes the architecture for the multi layered perceptron (MLP) that we used for the Physionet Challenge 2012 dataset. It is similar to the architecture used in Fortuin et al. [2019].

	Hyperparameter	Value
Inference network	Dimensionality of input	28×28
	Number of convolution layers	3
	Number of filters per convolution layer	72
	Kernel size	3×3
	Stride	2
	Number of feedforward layers	1
	Width of feedforward layers	128
	Dimensionality of latent space	L
	Activation function of layers	ELU
Generative network	Dimensionality of input	L
	Number of transposed convolution layers	3
	Number of filters per transposed convolution layer	72
	Kernel size	3×3
	Stride	1
	Number of feedforward layers	1
	Width of feedforward layers	128
	Activation function of layers	ELU

Table 1: Neural network architectures used in the Rotated MNIST dataset.

	Hyperparameter	Value
Inference network	Dimensionality of input	36×36
	Number of convolution layers	2
	Number of filters per convolution layer	144
	Kernel size	3×3
	Stride	2
	Pooling	Max pooling
	Pooling kernel size	2×2
	Pooling stride	2
	Number of feedforward layers	2
	Width of feedforward layers	300, 30
	Dimensionality of latent space	L
Generative network	Activation function of layers	RELU
	Dimensionality of input	L
	Number of transposed convolution layers	2
	Number of filters per transposed convolution layer	256
	Kernel size	4×4
	Stride	2
	Number of feedforward layers	2
	Width of feedforward layers	30, 300
	Activation function of layers	RELU

Table 2: Neural network architectures used in the Health MNIST dataset.

	Hyperparameter	Value
Inference network	Dimensionality of input	35
	Number of feedforward layers	2
	Number of elements in each feedforward layer	128, 64
	Dimensionality of latent space	L
	Activation function of layers	RELU
Generative network	Dimensionality of input	L
	Number of feedforward layers	2
	Number of elements in each feedforward layer	64, 128
	Activation function of layers	RELU

Table 3: Neural network architectures used in the Physionet Challenge 2012 dataset.

7 Supplementary images

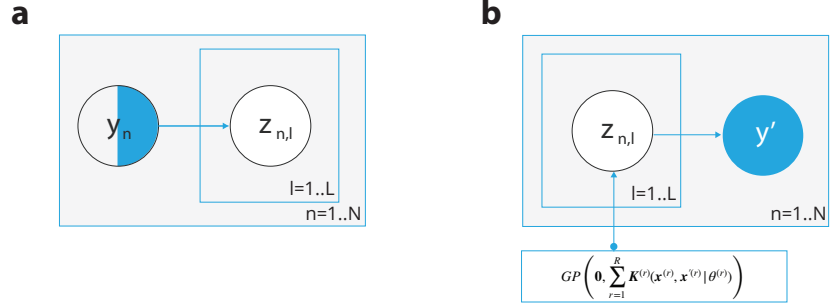


Figure 2: Plate diagram of the model. The shaded circle refers to an observed variable, the partially shaded circle refers to a partially observed variable (due to missing values), and the un-shaded circle refers to an un-observed variable. **(a)** Represents the inference (or encoder) model and **(b)** Represents the generative (or decoder) model.

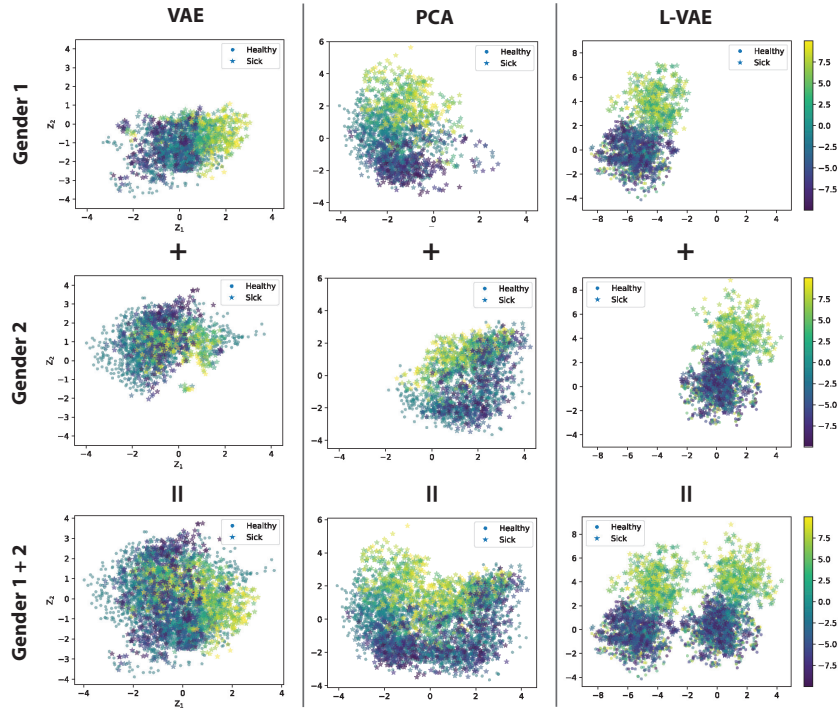


Figure 3: Comparison of the resulting latent space using VAE, PCA and, L-VAE on the Health MNIST dataset. The L-VAE model is fit using $f_{ca}(id) + f_{se}(age) + f_{ca \times se}(id \times age) + f_{ca \times se}(sex \times age) + f_{ca \times se}(diseasePresence \times diseaseAge)$ as the multi-output additive GP prior. The number of latent dimensions is set to 2. The points are coloured according to the diseaseAge as shown in the colour bar.

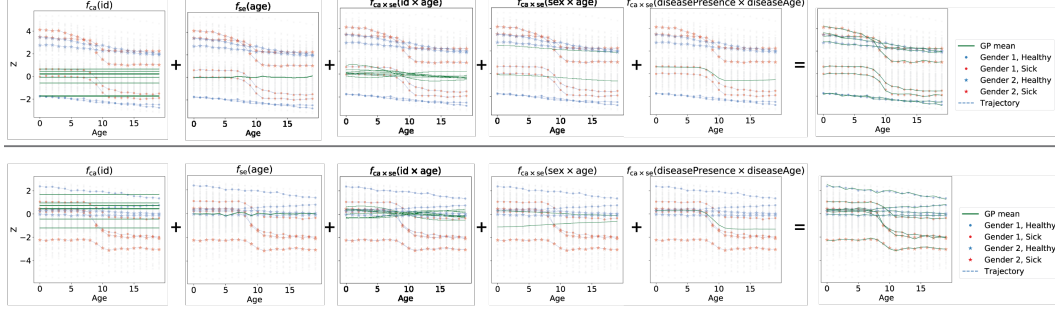


Figure 4: GP model fittings of L-VAE in the latent space with dimension 2 on the Health MNIST dataset.

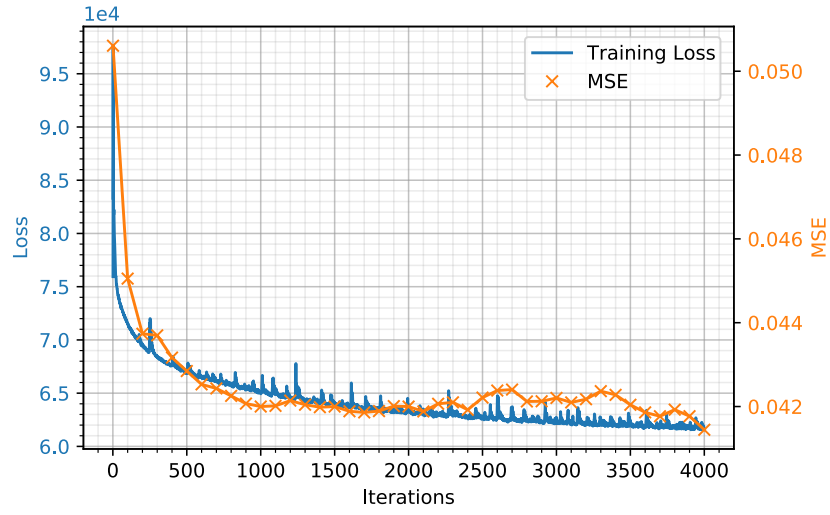


Figure 5: Visualisation of loss and MSE on test set for the Rotated MNIST experiment. The additive GP prior used is $f_{ca}(id) + f_{se}(angle) + f_{ca \times se}(id \times angle)$ and 16 latent dimensions.

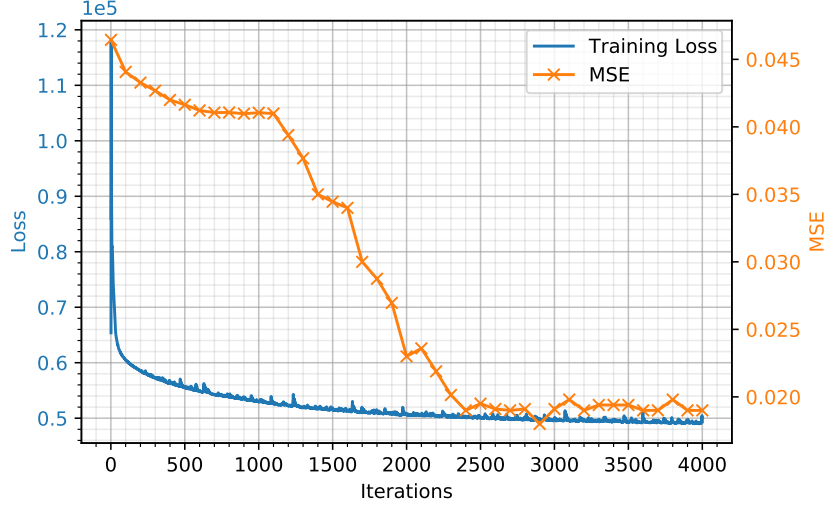


Figure 6: Visualisation of loss and MSE of imputed missing values for the Health MNIST experiment. The additive GP prior used is $f_{ca}(id) + f_{se}(age) + f_{ca \times se}(id \times age) + f_{ca \times se}(sex \times age) + f_{ca \times se}(diseasePresence \times diseaseAge)$ and 32 latent dimensions.

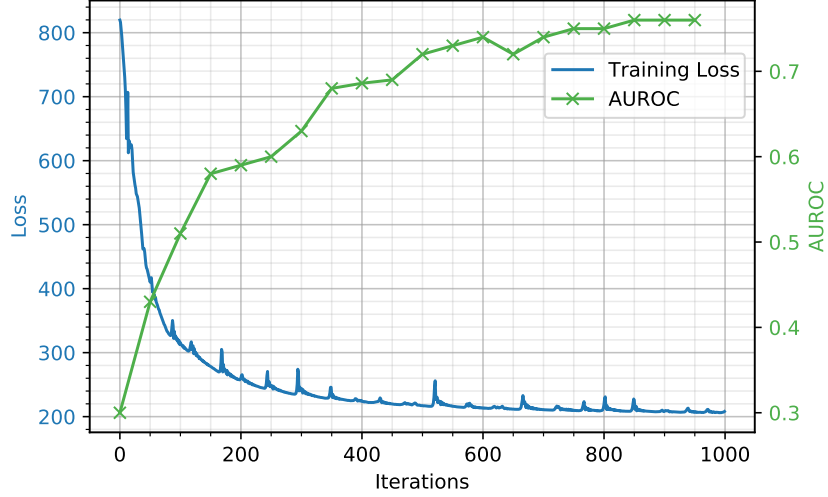


Figure 7: Visualisation of loss and AUROC for the classification task on the test set for the Healthcare data experiment. The additive GP prior used is $f_{ca}(id) + f_{se}(time) + f_{ca \times se}(mortality \times time) + f_{ca \times se}(sex \times time) + f_{ca \times se}(ICUtype \times time) + f_{ca \times se}(id \times time) + f_{ca \times se}(mortality \times mortalityTime)$ and 32 latent dimensions.

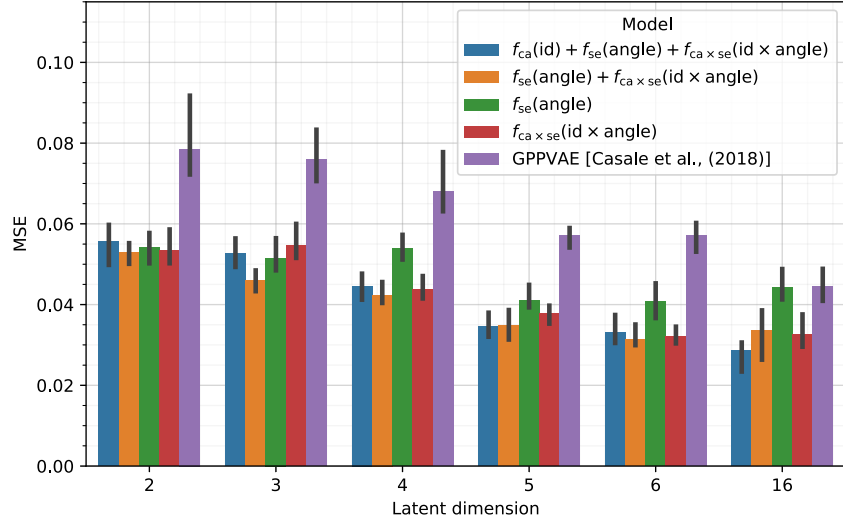


Figure 8: Comparison of MSE on the test set for the Rotated MNIST experiment using more configurations of L-VAE. It can be seen that the MSE performance is better when a more comprehensive additive kernel that utilises multiple auxiliary covariates is used.

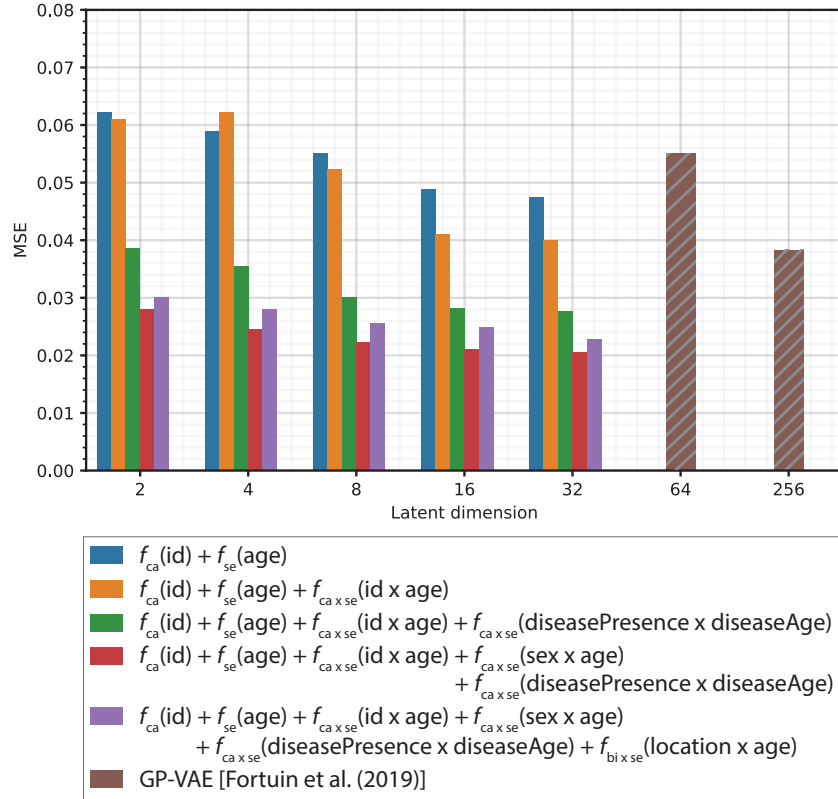


Figure 9: Comparison of MSE of the imputed missing values in the Health MNIST experiment using more configurations of L-VAE. The performance of L-VAE surpasses GP-VAE [Fortuin et al., 2019] when a multi-output additive GP prior with multiple auxiliary covariates is used. Moreover, it can be seen that L-VAE performs competitively even when simple multi-output additive GP priors are used with lower number of latent dimensions.

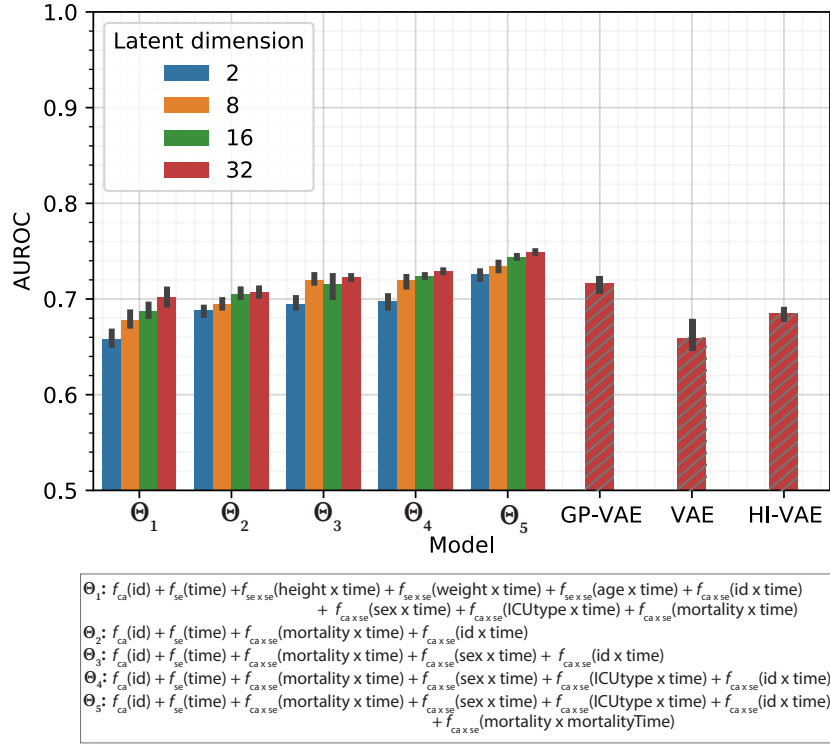


Figure 10: AUROC scores for the patient mortality prediction task on the test set of the Physionet Challenge 2012 dataset. This is an extension to fig. 4 in the main manuscript. In this figure, we can observe L-VAE’s performance with different latent dimensions as well as all the patient-specific general auxiliary covariates. Higher AUROC score is better.

References

- F. P. Casale, A. Dalca, L. Saglietti, J. Listgarten, and N. Fusi. Gaussian process prior variational autoencoders. In *Advances in Neural Information Processing Systems*, pages 10369–10380, 2018.
- L. Cheng, S. Ramchandran, T. Vatanen, N. Lietzén, R. Lahesmaa, A. Vehtari, and H. Lähdesmäki. An additive gaussian process regression model for interpretable non-parametric analysis of longitudinal data. *Nature communications*, 10(1):1–11, 2019.
- V. Fortuin, G. Rätsch, and S. Mandt. GP-VAE: Deep probabilistic time series imputation. *arXiv preprint arXiv:1907.04155*, 2019.
- I. Goodfellow, Y. Bengio, and A. Courville. *Deep learning*. MIT press, 2016.
- D. P. Kingma and J. Ba. ADAM: A method for stochastic optimization. *arXiv preprint arXiv:1412.6980*, 2014.
- D. P. Kingma and M. Welling. Auto-encoding variational bayes. *arXiv preprint arXiv:1312.6114*, 2013.
- A. Paszke, S. Gross, F. Massa, A. Lerer, J. Bradbury, G. Chanan, T. Killeen, Z. Lin, N. Gimelshein, L. Antiga, et al. PyTorch: An imperative style, high-performance deep learning library. In *Advances in Neural Information Processing Systems*, pages 8024–8035, 2019.
- W. H. Press, S. A. Teukolsky, W. T. Vetterling, and B. P. Flannery. *Numerical Recipes 3rd Edition: The Art of Scientific Computing*. Cambridge University Press, USA, 3 edition, 2007. ISBN 0521880688.
- M. Titsias. Variational learning of inducing variables in sparse gaussian processes. In *Artificial Intelligence and Statistics*, pages 567–574, 2009.
- C. K. Williams and C. E. Rasmussen. *Gaussian processes for machine learning*, volume 2. MIT press Cambridge, MA, 2006.